International Journal of Aeronautical and Space Sciences
https://doi.org/10.1007/s42405-024-00844-z

IJASS International Journal of Aeronautical and Space Sciences

ORIGINAL PAPER

On-orbit Thermal Analysis of CubeSat with CFRP Using Patterned Graphite Sheet and Stitching Method

Gyeong-Hun Bae[1] · Gyu-Beom Park[1] · Min-Kyu Kang[1] · Yong-Jin Jeon[1] · Byeong-Su Kwak[1] · Rho Shin Myong[1]

Received: 16 August 2024 / Revised: 8 October 2024 / Accepted: 23 October 2024

Abstract
Satellites operate in a space thermal environment and can suffer from extreme temperature variations. To survive and perform missions within the mission period, a thermal control system must be applied. These thermal control systems quickly disperse heat and evenly distribute heat between components to keep the temperature of the satellite's internal components within the allowable temperature range. Aluminum, which is predominantly used in satellite frames for its excellent thermal conductivity, serves as an efficient thermal transfer path with advantageous thermal conductivity. However, its relatively high density increases the satellite's overall weight and makes it hard to meet the recent demand for miniaturization and weight reduction in artificial satellites. Alternatively, carbon fiber composites can potentially be used in the space environment, replacing aluminum to achieve weight reduction. However, such composites have relatively low thermal conductivity, making them unsuitable for use as a heat transfer path. In this study, to solve this problem, a carbon fiber composite material with improved thermal performance was produced using a patterned graphite sheet and stitching method, and thermal properties were measured. The implemented composite was applied to a solar panel of a 3U cube satellite model, which was designed using a Thermal Desktop, weighing approximately 3.7 kg. Orbital thermal analysis was performed with SINDA/FLUINT to analyze its thermal performance in space environments, and the analysis results were compared and analyzed. This study proposes a new carbon fiber composite material capable of weight reduction and effective heat control.

Keywords Carbon fiber-reinforced plastic · Graphite sheet · Stitching · CubeSat · Thermal design and analysis

1 Introduction

Satellites operating in the vacuum environment of space face extreme high and low temperatures. Because each system mounted on a satellite has a specific operating temperature range, an appropriate thermal design is needed to ensure that it meets that range [1, 2]. Satellites and solar panels are affected by solar radiation, the Earth's albedo, and IR radiation energy in orbit. Simultaneously, they are exposed to the extreme environment of deep space, including temperatures of – 270° [3–7]. In particular, when solar panels equipped with solar cells are exposed to the most severe high- and low-temperature environments, the temperature of the solar cells may surge or drop excessively, causing a reduction in power generation efficiency. Therefore, having a thermal design that can minimize changes in cell temperature is essential [8, 9]. As a thermal control technique to maintain the operating temperature range of CubeSat components and solar panels, a passive thermal control technique is mainly used. The arrangement consumes little power and is highly space-efficient. [10]. When the thermal conductivity of a solar panel is increased in the thickness direction, it allows heat to be effectively dispersed through the panel and discharged into deep space. Thus, the thermal conductivity of a solar panel is one of the important factors in its thermal design.

To achieve CubeSat's lightweight and small volume, printed circuit board (PCB)-based solar panels have been widely used to enhance electric circuit design and reduce weight [11]. Overseas CubeSat-related companies with space mission experience, such as EnduroSat, Andrews Space, and Pumpkin, provide PCB-based solar panels for CubeSat. However, the PCB structure has multiple insulation and

Communicated by Kyung-Su Na.

✉ Rho Shin Myong
myong@gnu.ac.kr

[1] School of Mechanical and Aerospace Engineering, Gyeongsang National University, 501 Jinju-Daero, Jinju 52828, Gyeongnam, Republic of Korea

Published online: 07 December 2024

copper layers. The low thermal conductivity of the insulator hinders solar cell heat release due to the low thermal conductivity in the thickness direction [12]. In addition, if the thickness of the PCB is reduced to improve heat dissipation performance, the panel's rigidity will be diminished, making it difficult to guarantee the solar cell's structural stability in a vibrating launch environment. Consequently, solar panels have been developed by attaching solar cells to aluminum-based solar panels without using PCBs [6, 13–17]. The use of aluminum materials avoids structural and thermal problems; however, the relatively high density of aluminum increases the weight of the solar panel. Consequently, this approach may conflict with the growing demand for miniaturization and weight reduction to reduce the launch and development cost of satellites [18].

In the aerospace sector, the use of highly integrated electronics has expanded to improve performance and achieve miniaturization and weight reduction [19, 20]. However, high-density packaging generates a large amount of heat per unit area [21], and the subsequent thermal load can degrade the performance of the electronic equipment. Accordingly, to ensure the effective operation of satellite systems, effective thermal control systems and materials with high thermal conductivity are necessary [22–25].

While aluminum alloys are mainly used as high-thermal-conductivity materials, carbon fiber composites have recently attracted attention as materials suitable for miniaturization and weight reduction [14, 26–33]. Carbon fiber composites can be employed in extreme space environments because of their lightweight and low thermal expansion coefficients, high specific strength, and specific stiffness [34–37]. However, their low thermal conductivity compared to aluminum limits their use for thermal control. Consequently, studies have been conducted on carbon fiber composites based on graphite sheets (GS) [38], a material with high thermal conductivity, and pitch-based carbon fibers [39]. However, because of their nature, graphite sheets have particularly low strength in the thickness direction. Delamination may even occur under a small load when inserted into carbon fiber-reinforced plastic (CFRP).

In this study, a composite with three-dimensional (3D) heat transfer paths was implemented using a patterned graphite sheet (PGS). The PGS has excellent thermal properties and complements the limitations of graphite and pitch-based carbon fibers which provide high thermal conductivity only in the fiber direction. Its thermal properties were measured and an on-orbit thermal analysis was conducted to investigate the use of the composite in a solar panel of a 3U CubeSat, to verify its thermal performance in the space environment. Then, the results were compared and analyzed. Consequently, a new carbon fiber composite is proposed that can achieve both weight reduction and effective thermal control.

2 Composites with Improved Thermal Conductivity

2.1 Material Selection

Table 1 summarizes previous studies that have employed various materials (Aluminum, CFRP, etc.) in the solar panels of satellites. These include recent research on the thermal conductivity, specific heat, and density of various materials used in satellite solar panels. In the table, it can be observed that aluminum exhibits high thermal conductivity but suffers from high density. CFRP is challenged by its very low thermal conductivity.

In this study, PAN-based carbon fiber/epoxy composites with improved heat transfer performance were designed and implemented. The PAN-based carbon fiber/epoxy used was Toray's WSN 03KP 200 Y K51M product. To improve the in-plane thermal conductivity of the PAN-based carbon fiber/epoxy composites, G&CS Co., Ltd.'s GP-0025 product was used as GS. GS has a high thermal conductivity in the in-plane direction of approximately 1400 W/m·K and was used to improve in-plane thermal conductivity by laminating it within a composite material.

To improve the through-thickness thermal conductivity of the PAN-based carbon fiber/epoxy composites, Nippon Graphite Fiber Co., Ltd.'s XN-90-60S product was used as the pitch-based carbon fiber. Pitch-based carbon fiber has a high thermal conductivity of approximately 500 W/m·K in the fiber direction, and stitching was used to improve thermal conductivity in the thickness direction.

2.2 Composite Design

Figure 1 describes a conceptual diagram of the implemented composite to illustrate the geometrical structure. GS or PGS and pitch-based carbon fiber were applied to the PAN-based carbon fiber/epoxy composites. This formed a continuous heat transfer path in the in-plane and through-thickness direction of the composite material, significantly increasing the thermal conductivity of the composite material. However, GS is formed by van der Waals interactions in the thickness direction, which results in weak interface characteristics.

PGS can improve thermal conductivity without interrupting continuous heat transfer paths. The pattern of the PGS can improve the adhesion area between laminar carbon fibers. In this way, it can enhance the low interface characteristics of the GS and prevent the delamination of the implemented composite. In this study, PGS was laminated on the PAN-based carbon fiber/epoxy composite, and pitch-based carbon fiber was stitched. As a result, a composite material with improved thermal conductivity was realized by forming a continuous heat transfer path in the plane and thickness directions of the composite material.

Table 1 Review of literature on the thermal properties of materials used in satellite solar panels

References	Applied component location	Material	Thermal conductivity [W/m·K]	Specific heat [J/g·K]	Density [kg/m^3]
Shin et al. [14]	Solar Panel (Face sheet)	Al-2024-T3	121	921	2768
Abdelal et al. [32]	Solar Panel (Face sheet)	Composite (per layer)	4.15	1884	–
Li et al. [33]	Solar Panel (Face sheet)	CFRP	k_{xx}: 6.2334 k_{yy}: 0.6935 k_{zz}: 0.6935	836	–
Khalifa et al. [6]	Solar Panel	Al-7075-T6	130	960	2810
Almehisni et al. [15]	Solar Panel (Thermal Path)	Al-6061-T1	154.25	896	2711
		Titanium (Ti-6Al-4 V)	6.7	526	4430
		G10	0.288	1400	2100
Park et al. [16]	Solar Panel	Al-7075	121.2	961.2	2770
		CFRP	30	711.76	1910
Bhattarai et al. [11]	Solar Panel	PCB-Cu4.6%	0.29	1544	1850
Budiantoro et al. [17]	Solar Panel (Face sheet)	Carbon fiber (M55J)	156	712	712
		Aluminum alloy 7075-T651	130	960	2810
Present	Solar Panel	CFRP (PGS_P7_S)	k_{xy}: 34.203 k_z: 38.731	886	1614

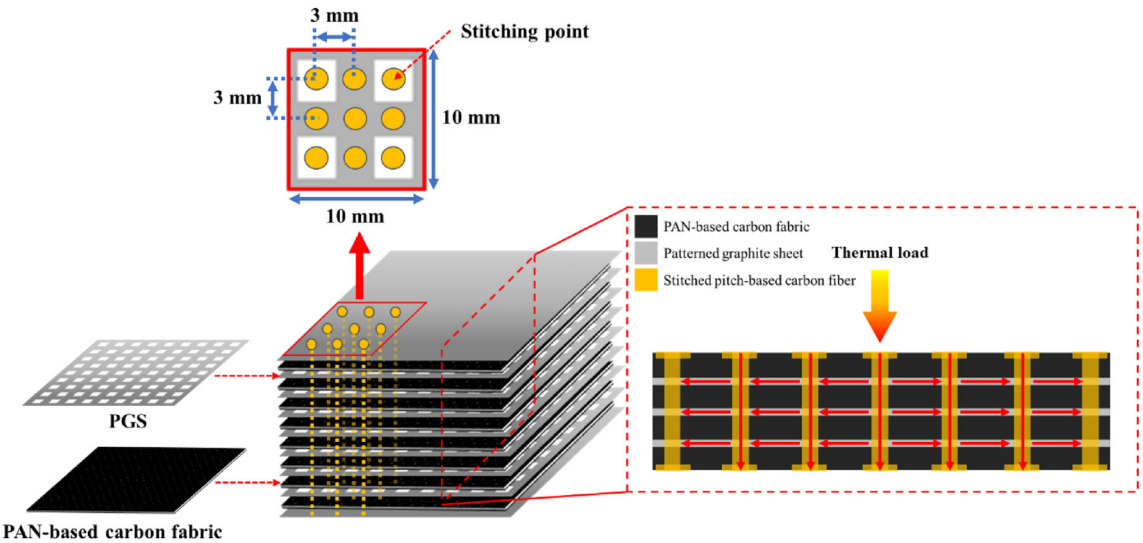

Fig. 1 Conceptional diagram of carbon/epoxy composite with improved thermal conductivity PGS_P7_S

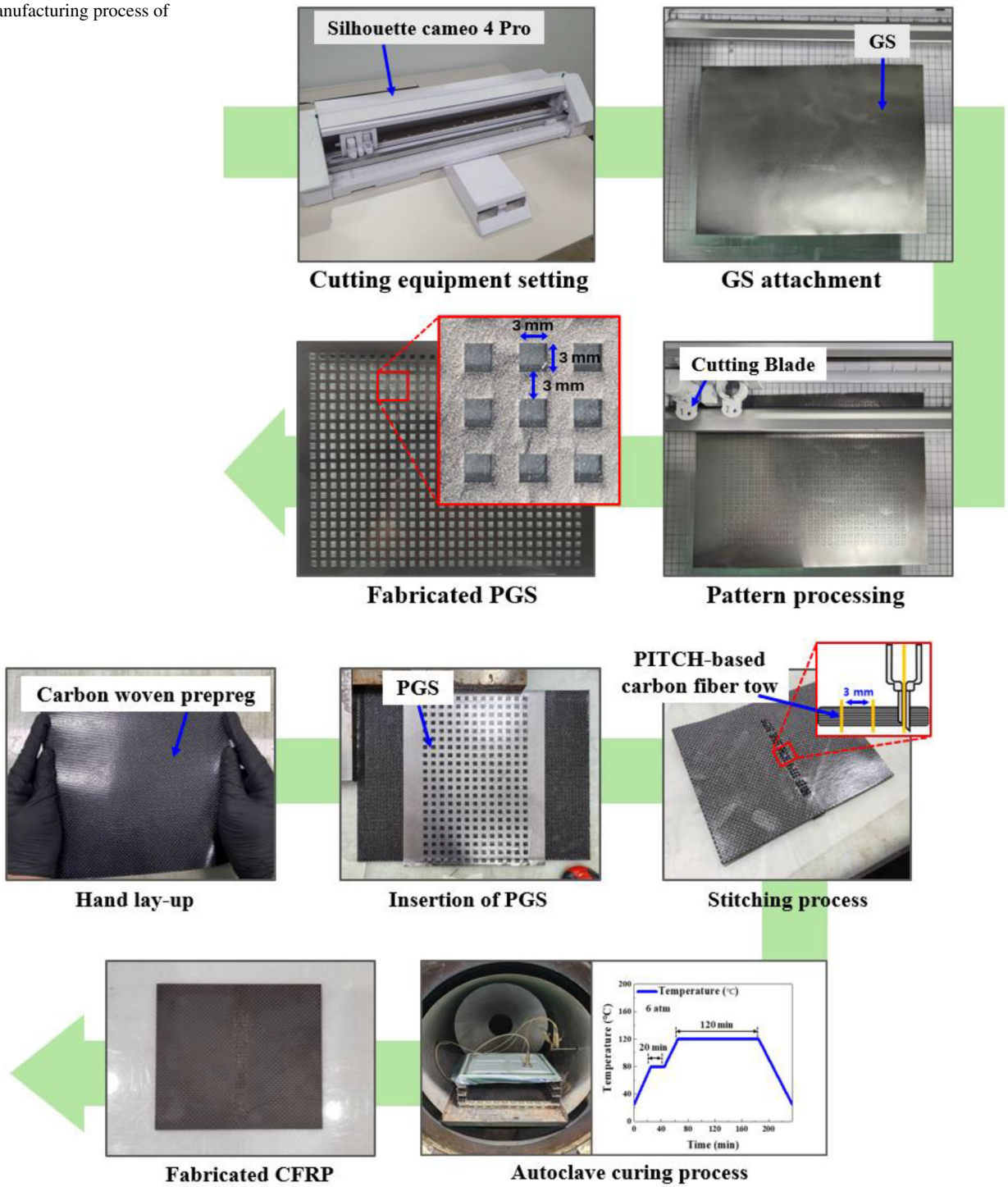

Fig. 2 Manufacturing process of PGS

Fig. 3 Composite manufacturing process with improved thermal conductivity

2.3 Manufacturing Process

Figure 2 presents the PGS manufacturing process. PGS was manufactured using Silhouette's Cameo 4 Pro equipment. After attaching the film-protected GS to the 600 mm × 600 mm cutting mat of the Cameo 4 pro equipment, the pattern was processed automatically as indicated in the drawing. PGS was acquired by removing an array of square-patterned areas from the cutting mat. The square pattern in the manufactured PGS was 3 mm × 3 mm, and the gap between the patterns was 3 mm.

The composite with improved thermal conductivity was manufactured using a geometric design, and the manufacturing process is shown in Fig. 3. GS, or PGS, was stacked between the carbon fiber prepreg layers. A 3 mm-interval stitching process [40] was applied to insert pitch-based carbon fibers using a 1.8 mm-diameter stainless-steel needle to penetrate the laminated composite.

To ensure precise positioning and spacing of pitch-based carbon fiber during the stitching process, a guide was prepared by machining holes into a 2 mm-thick acrylic plate. The guide was placed on both the top and bottom of the laminate and passages in the through-thickness direction were created using a stainless-steel needle with a diameter of 1.8 mm. Subsequently, the pitch-based carbon fiber was inserted into the passages formed by the needle, and the needle was carefully removed. Upon removal of the needle, the fibers were cut, thereby completing the stitching process.

The laminated plate manufactured above was subjected to vacuum bagging and hardened through autoclave curing. Manufacturing was completed by applying a pressure of 6 atm and a curing cycle of 20 min at 80 °C and 120 min at 120 °C.

A total of three panels were fabricated: a panel that stacked eight layers of the carbon fiber prepreg (Pristine) and panels that employed 3 mm-interval stitching after stacking GS or PGS between each prepreg layer (GS_P7_S and PGS_P7_S). 'Pristine' refers to PAN-CFRP without the application of GS or stitching, while 'S' indicates the implementation of a stitching process using pitch-based carbon fiber. 'GS' or 'PGS' denotes the insertion of GS or PGS within the laminate, and 'P7' specifies that seven sheets are inserted. The specimens were processed into 10 mm × 10 mm sizes for thermal conductivity measurement.

2.4 Measurement of the Thermal Properties of Composites

Specific heat and thermal diffusivity were measured to confirm the thermal properties of the composite material implemented in this study. Thermal conductivity is calculated using Eq. (1)

$$\lambda = \rho \cdot \alpha \cdot c_p, \tag{1}$$

where λ is the thermal conductivity (W/m·K), ρ is the density (kg/m^3), α is the thermal diffusivity (mm^2/s), and c_p is the specific heat (J/g·K). The density of each specimen (ρ) was derived by measuring its volume and weight. Mettler—Toledo's electronic microbalance XSR205 product was used to measure the weight, and the volume was calculated by measuring the width, height, and depth using a micrometer. The apparent density was calculated using the measured weight and volume of the specimen. The specific heat of the specimen was measured using NETZSCH's DSC 204 F1 Phoenix equipment. The enthalpy difference was obtained through the temperature difference between the standard sample of mass and the specimen under a heating rate of 10 °C/min from – 10 to 50 °C. In this way, the specific heat was measured. NETZSCH's LFA-467 equipment, which utilizes the laser flash analysis method (LFA), was used for thermal diffusivity measurement per the ASTM E1461 standard [41]. The specific heat was measured with the above process, and thermal conductivity was derived for the three specimens mentioned above.

Table 2 and Fig. 4 show the measurement results of the carbon fiber composites with improved thermal conductivity. On-orbit thermal analysis was conducted by applying the measurements to the solar panel of the 3U CubeSat.

Table 2 Thermal properties of the materials used for analysis

Specimen ID	Specific heat [J/kg·K]	Thermal conductivity [W/m·K]	
		Through-thickness	In-plane
Pristine	906	0.59	2.32
GS_P7_S	890	33.12	29.21
PGS_P7_S	886	38.73	34.20
AL_6061 [42]	961	167.90	167.90

2.5 Mechanical Test of Composites

Tensile tests were conducted to evaluate the mechanical properties of composites enhanced for thermal conductivity using PGS and stitched fibers. The equipment used for the test was the FXYB305C from MTS, and the test was performed in accordance with the relevant standard, ASTM D3039 [43]. Additionally, to prevent damage at the grip section during the tensile test, tabs were attached to the specimens before testing. The specimen size was set to 250 mm × 30 mm to

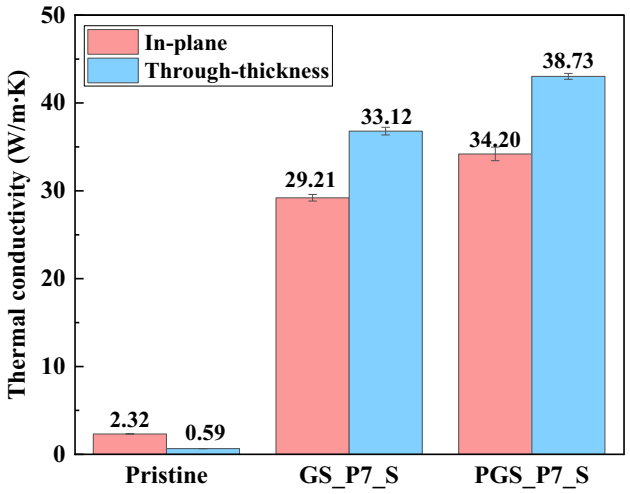

Fig. 4 Thermal conductivity measurement results using the LFA method

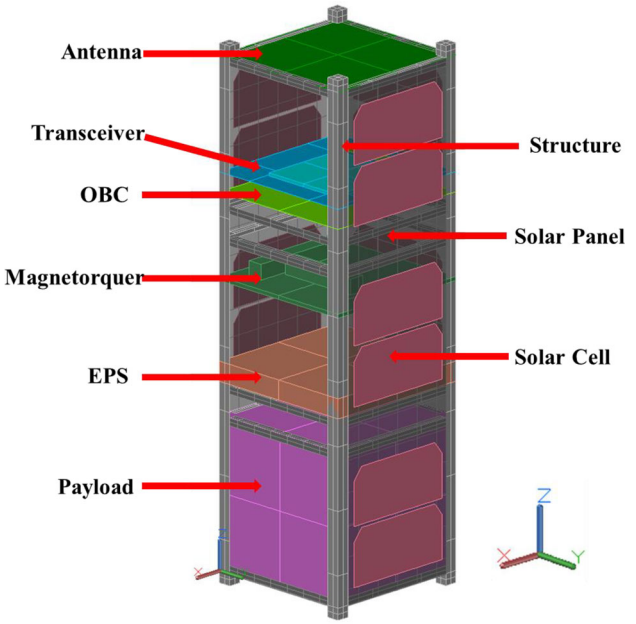

Fig. 5 3U CubeSat thermal model

ensure the same number of patterns within the PGS for all specimens. According to the ASTM standard, the load speed for the tensile test was set at 1.3 mm/min, and the load was applied until specimen failure.

Tensile tests were conducted on Pristine and PGS_E1_S specimens. The measured data were obtained using the average of five specimens. The results indicated that the strength and stiffness of the Pristine were 702 MPa and 63.9 GPa, respectively, whereas the PGS_E1_S showed a strength of 242 MPa and a stiffness of 39.5 GPa.

3 On-orbit Thermal Analysis of CubeSat

3.1 Energy Equation and Numerical Analysis

The energy equation of the heat model applied to systems operating in space for thermal analysis is an energy equation that excludes the convection term, as shown in Eq. (2) [44]

$$\rho c \frac{\partial T}{\partial t} = \nabla \cdot (k \nabla T) + \dot{Q}''' - \nabla \cdot (q_r). \tag{2}$$

The first term on the right side is the calculation term by conduction, and the second is by boundary surface radiation. Boundary surface radiation includes the CubeSat surface and solar radiation, albedo, and the space thermal environment caused by Earth's radiation. The last term consists of the heat released from equipment, internal heat of devices (e.g., heaters), and heat absorbed from the external boundary.

For the above energy equation, SINDA/FLUINT, a commercial thermal analysis software program, performs calculations using the Crank–Nicholson method based on numerical analysis, as shown in Eq. (3) [45]

$$\begin{aligned} &\frac{2C_i}{\Delta t}(T_i^{n+1} - T_i^n) = 2Q_i + \\ &\sum_{j=1}^{N}[G_{ji}(T_j^n - T_i^n) + \hat{G}_{ji}\{(T_j^n)^4 - (T_i^n)^4\}] + \\ &\sum_{j=1}^{N}[G_{ji}(T_j^{n+1} - T_i^{n+1}) + \hat{G}_{ji}\{(T_j^{n+1})^4 - (T_i^{n+1})^4\}], \end{aligned} \tag{3}$$

where T_j is the node temperature of the present time t, T_j^{n+1} is the node temperature after Δt from the present time, G_{ji} is the value connected with the linear conductors of the diffusion nodes j and i, $\hat{G}_{ji}$ is the radiation conductor, C_i is the thermal capacity of the node i, and Q_i is the heat source. The above equation that used the Crank–Nicholson method is repeatedly calculated until T_{n+1} converges as follows [45]:

$$|T_j^{(l+1)} - T_j^{(l)}|^{\overline{\kappa}} < \varepsilon^*, \tag{4}$$

where l and $\overline{k}$ are the iteration level and the time step, respectively. ε^* is the convergence area. The thermal mathematical model (TMM) used for the analysis of the temperature distribution is a numerical analysis software program that uses the finite difference method (FDM) after modeling each component of the satellite by dividing them into nodes and making a heat transfer governing equation in a simple form. This

Table 3 Optical properties

Component	Location	Absorptivity (α)	Emissivity (ε)
Aluminum 5754	STR	0.160	0.030
PCB*4.6%Cu	PCBs	0.810	0.900
GaAs	Solar Cell	0.920	0.850
C11000	Transmitter	0.320	0.020
Anodize, black	Solar Panels	0.880	0.880
	Antenna		
Tape, 850-3 M Aluminized mylar	EPS	0.150	0.590
Antenna	Antenna	0.356	0.87
MLI top		0.49	0.83
MLI bottom		0.15	0.02

method has been widely used in thermal analysis research, because it involves simple calculations and is in good agreement with the analysis solution as the node size decreases [46].

3.2 Satellite Thermal Model

The micro-satellite used in this study was simplified based on the 3U structure provided by ISISPACE and designed as shown in Fig. 5 [47]. TMM was constructed on a Thermal Desktop, facilitating finite difference and finite element models. The solar panels and solar cells were installed on five sides other than the satellite payloads, and the + Z Panel with an antenna was used to perform missions. Here, it was assumed that the backing material determined the thermophysical and optical properties of the solar panel.

In addition, to compare accurate thermal properties according to the thermal conductivity of the four different solar panels, which were prepared with materials with different thermal conductivities, black anodizing was applied to the internal and external optical properties of the solar panel in all cases. Tables 3 and 4 provide the optical and thermophysical properties applied to the thermal model of the CubeSat, respectively.

The thermal conductance between the satellite payloads and the panels was simulated using a conductor, and 1,342 nodes were applied to the thermal model.

Because the antenna is directly exposed to the space environment, it was designed to be less affected by the radiant energy from the environment by applying a multi-layer insulator (MLI).

The solar panels were designed on the side panel that surrounds the satellite ($X+$, $X-$, $Y+$), the side panel where the radiator is located ($Y-$), and the bottom panel ($Z-$). The related parameters are shown in Table 5. The mass of the 3U CubeSat according to the material applied to the solar panels was derived from Table 5, and the results are shown in Table 6.

The mass of the solar panel with Aluminum6061-T6 was 0.771556 kg, while the masses of the Pristine, GS_P7_S, and PGS_P7_S solar panels were 46.2%, 43.4%, and 40.4% lower (0.414818, 0.436456, and 0.459517 kg), respectively.

Table 4 Thermophysical properties

Material	Conductivity [W/m·K]		Density [kg/m^3]	c_p [J/kg·K]
	k_{xy}	k_z		
Aluminum 6061-T6	167.9	167.9	2710	961
Aluminum 5754	125	125	2670	961
PCB-4.6%Cu	18.04	18.04	2259.77	1544.11
Li_Po	2.49	2.49	3115	601
PEEK	0.25	0.25	1320	1700
C11000	391.2	391.2	8860	385.2
GaAs	46.05	46.05	5320	350
Payload lumped	18.04	167.9	1953	963.8
EPS lumped	18.04	0.0249	2509	654.36
Solar Panel	167.9	167.9	2842.52	900.75
	2.320	0.590	1457	906
	29.207	33.115	1533	890
	34.203	38.731	1614	886
Magnetorquer	391.2	391.2	8660	1882.8
Kapton HN	0.12	0.12	1420	1093

Table 5 Solar panel parameters

Components	Length [cm]	Width [cm]	Thickness [cm]	Area [cm^2]	Volume [cm^3]
Side panel ($X+$, $X-$, $Y+$)	32.54	8.3	0.25	270.082	67.5205
Side panel ($Y-$)	27.54	8.3	0.25	228.582	57.1455
Bottom panel ($Z-$)	10	10	0.25	100	25

Table 6 Solar panel volume and total mass

Panel material	Total volume of panel [cm^3]	Density [kg/cm^3]	Total mass of panel [kg]	Total mass of 3U CubeSat [kg]
Pristine	284.707	0.001457	0.414818	3.357841
GS_P7_S		0.001533	0.436456	3.379479
PGS_P7_S		0.001614	0.459517	3.402540
Aluminum6061-T6		0.002710	0.771556	3.714579

Table 7 Orbit definition

Parameter	Orbit condition	
	Worst cold	Worst hot
Orbit type	Sun-synchronous	
Inclination angle [deg]	98.13	
Altitude [km]	685	
Period [sec]	5907.55*10	
Orientation	Nadir-Pointing ($-Z$ axis earth center-pointing)	
Solar Flux [W/m^2]	1287	1420
Albedo	0.30	0.35
IR Flux [W/m^2]	227	249
Right ascension of sun [deg]	90 [Summer]	270 [Winter]

The satellite's total mass was reduced by 9.60%, 9.02%, and 8.40%, respectively, compared to the solar panel that applied Aluminum6061-T6. These results confirmed the composite material implemented in this study reduced the weight.

3.3 Thermal Analysis Conditions

For a satellite to perform missions successfully in a space environment with extreme temperature differences, the thermal design must ensure that the payloads and all components can withstand the worst low and high temperatures in the mission orbit. Table 7 shows the orbit and thermal environment conditions applied in the thermal analysis.

The in-orbit thermal analysis was conducted for the four cases under the worst conditions. First, the case where the in-orbit thermal environment in the mission mode of the CubeSat is the winter solstice was defined as Cold Operational, and the case where it is the summer solstice was designated Hot Operational. The data for the main missions were collected using the main mounted equipment. The case where the on-orbit thermal environment is in emergency mode (the case with the smallest heat release in the event of a problem with the satellite, while operating minimum units) was the summer solstice, and defined as Cold Survival. The case where the on-orbit thermal environment in the transmission mode (the case with the most significant heat release as the satellite transmits data to the Earth) is the winter solstice,

Table 8 Heat loads

Submodel	Cold case operational [W]	Cold case survival [W]	Hot case operational [W]	Hot case transmit [W]
Antenna	0.04	0.00	0.04	0.04
EPS	0.13	0.01	0.13	0.13
Magnetorquer	1.20	0.18	1.20	1.20
OBC	0.40	0.40	0.40	0.40
Payload	0.00	0.00	2.00	0.00
Transceiver	0.48	0.00	0.48	4.00
Total	2.25	0.59	4.25	5.77

and is defined as Hot Transmit. In addition, six heat loads were applied to the onboard computer (OBC), transmitter, magnetorquer, electrical power system (EPS), antenna, and payload to implement the heat released from the internal payload from the mission. Table 8 shows the applied heat loads.

4 Thermal Analysis Results

The thermal properties of the CubeSats with the carbon fiber composite materials in this study were compared. To compare thermal properties, orbital thermal analysis was performed using SINDA, a commercial thermal analysis program. The results for the three cases of carbon fiber composites and the temperature characteristics of the satellite fabricated with Aluminum 6061-T6 were compared and analyzed.

Tables 9 and 10 summarize the allowable temperature range and thermal analysis results for all components in the worst case by material. The temperatures of each component in the mission and transmission modes analyzed under high-temperature conditions are shown as the Worst Hot Case in Table 9. The low-temperature analysis results of each component calculated in the mission and the emergency modes for summer solstice are summarized as the Worst Cold Case in Table 10. In this way, it was possible to examine whether the worst temperature case for each satellite mode met the allowable temperature conditions of each component according to the solar panel material that was used. In addition, the tendency in the temperature distribution of the satellite was determined, for each material and mode.

4.1 Worst Hot Case of Solar Panel (+ X)

The temperature results in Table 9 show that all of the components of the satellite met the operating temperature requirements for the mission and the transmission modes for all materials. The transceiver had the largest heat release compared to other components and exhibited the highest maximum temperature in the Hot Transmit Case, which was the transmission mode. As shown in Table 9, the maximum temperature was 50.9 °C when the Pristine case was considered. In addition, for GS_P7_S and PGS_P7_S, the maximum temperatures of 48.2 °C and 47.9 °C were observed, which were 2.7 °C and 3 °C lower compared to Pristine. This indicates that the improved thermal properties of the materials in the solar panel efficiently dispersed the heat generated inside the satellite and affected the temperature ranges of components by promoting heat release into deep space.

Figure 6 shows the temperature distribution of the solar panels and solar cells in Hot Transmit, where the heat released from the components was the largest, and the in-orbit thermal environment was the winter solstice. Figure 7 compares the temperature distributions in the solar panels with the three composites and the aluminum-based solar panel when the solar cell showed the maximum temperature. First, it was found that the maximum and minimum temperatures of the solar panels for all cases derived from the thermal analysis results met the allowable temperature range (− 40–120 °C). As shown in Figs. 6 and 7, the maximum temperatures of the solar cell and solar panel were the highest when Pristine was considered, and its temperature range was the largest among the four cases. While the maximum temperature of the solar panel was 74.5 °C, the maximum and minimum temperatures of the solar cell were 76.3 °C and 44.2 °C, respectively. The solar panels with GS_P7_S and PGS_P7_S showed maximum temperatures of 62.9 °C and 61.8 °C, respectively, as shown in Figs. 6 and 7. Here, the maximum and minimum temperatures of the solar cells with GS_P7_S were 65.6 °C and 35.0 °C, respectively. These were 10.7 °C and 9.2 °C lower compared to Pristine, respectively. The maximum and minimum temperatures of the solar cells with PGS_P7_S were 64.5 °C and 33.2 °C, respectively. These were 11.8 °C and 9.2 °C lower compared to Pristine, respectively. The maximum temperature of the aluminum-based solar panel was 48.1 °C. In that case, the maximum and minimum temperatures of the solar cell were 51.5 °C and 30.9 °C, respectively, which was the shortest temperature range.

4.2 Worst Cold Case of Solar Panel (+ *Y*)

The temperature results in Table 10 show that the EPS deviated from the minimum temperature requirement of − 0.3 °C in emergency operation mode with Pristine, and the transceiver deviated from the minimum temperature requirement in emergency operation mode for all materials. The payload could not meet the allowable temperature range in the mission and emergency modes with any of the materials as it exceeded the lowest temperature requirement. For these components, it is judged that an additional thermal design will be required, such as the application of MLI or heaters.

In addition, it was found that the temperature range of the components was reduced when GS_P7_S and PGS_P7_S were applied, compared to the Pristine case. This indicates that the thermal properties of the material used in the solar panel affect the temperatures of the components inside the satellite.

Figure 8 shows the temperature distribution in the solar panel and the solar cell in Cold Survival, where the heat release from the components was small, and the in-orbit thermal environment was the summer solstice. Figure 9 compares the temperature distributions in the solar panels for the three cases of composites and the aluminum-based solar panel when the solar cell exhibited the minimum temperature.

As shown in Figs. 8 and 9, the minimum temperatures of the solar cell and solar panel were lowest for the Pristine case,

Table 9 Orbital thermal analysis results in hot case

Components	Operating temp [°C]		Analysis temp. [°C]															
	Material		Pristine				GS_P7_S				PGS_P7_S				AL_6061			
	Min	Max	Worst hot															
			Operational		Transmit		Operational		Transmit		Operational		Transmit		Operational		Transmit	
			Min	Max	Min	Max	Min	Max	Min	Max	Min	Max	Min	Max	Min	Max	Min	Max
Antenna	− 20	60	− 2.3	46.9	7.0	55.2	− 1.1	46.5	8.8	56.5	− 1.0	46.4	7.9	54.9	0.9	45.8	7.6	51.6
EPS	− 20	70	− 4.1	14.7	− 3.6	15.1	− 4.0	14.2	− 2.5	15.6	− 4.0	14.1	− 2.4	15.6	− 3.5	14.0	− 1.0	16.5
Magnetorquer	− 40	70	− 3.8	15.8	2.6	22.0	− 4.1	15.9	1.7	21.4	− 4.0	15.8	1.7	21.3	− 2.5	14.9	2.2	19.5
OBC	− 25	65	− 6.6	20.8	7.0	35.6	− 5.8	19.7	6.4	33.3	− 5.7	19.5	6.4	33.0	− 3.0	17.7	7.3	29.6
Payload	− 10	50	1.4	10.4	− 1.7	7.4	0.4	10.5	− 0.6	9.4	0.3	10.5	− 0.5	9.6	− 0.1	10.8	1.0	11.8
Solar Cell	− 100	100	− 20.9	70.8	− 12.9	76.3	− 16.9	60.1	− 9.8	65.6	− 16.5	59.0	− 9.5	64.5	− 11.8	47.1	− 7.0	51.5
Solar Panel	− 40	125	− 25.9	68.9	− 26.0	74.5	− 25.3	57.2	− 25.4	62.9	− 24.9	56.1	− 25.1	61.8	− 19.0	43.5	− 18.9	48.1
Structure	− 40	80	− 17.5	55.4	− 10.3	62.4	− 16.1	53.0	− 8.7	59.1	− 15.7	52.2	− 8.5	58.3	− 11.0	45.9	− 6.1	51.8
Transceiver	− 20	60	− 10.5	26.7	− 0.2	50.9	− 9.6	25.6	− 0.8	48.2	− 9.4	25.3	− 0.7	47.9	− 6.5	22.1	0.5	44.1

Table 10 Orbital thermal analysis results in cold case

Components	Operating temp [°C]		Analysis temp. [°C]													
	Material		Pristine				GS_P7_S				PGS_P7_S				AL_6061	
	Min	Max	Worst cold													
			Operational		Survival		Operational		Survival		Operational		Survival		Operational		Survival	
			Min	Max	Min	Max	Min	Max	Min	Max	Min	Max	Min	Max	Min	Max	Min	Max
Antenna	− 20	60	− 8.3	36.4	− 13.6	31.5	− 6.3	37.3	− 12.3	31.6	− 7.4	35.6	− 12.7	30.9	− 7.1	34.0	− 11.3	30.7
EPS	− 20	70	− 16.0	1.4	− 20.3	− 2.7	− 15.3	1.4	− 19.6	− 2.7	− 15.2	1.4	− 19.5	− 2.8	− 14.5	1.6	− 18.8	− 2.6
Magnetorquer	− 40	70	− 13.6	4.3	− 20.0	− 2.2	− 13.8	4.3	− 19.8	− 1.9	− 13.7	4.2	− 19.7	− 1.9	− 12.8	3.0	− 18.3	− 2.9
OBC	− 25	65	− 15.3	9.7	− 21.6	3.6	− 14.8	8.5	− 20.7	2.5	− 14.7	8.3	− 20.6	2.2	− 12.9	5.8	− 18.3	0.3
Payload	− 10	50	− 13.1	− 4.9	− 16.6	− 8.3	− 12.8	− 3.6	− 16.5	− 7.3	− 12.7	− 3.5	− 16.4	− 7.2	− 12.3	− 2.5	− 16.3	− 6.4
Solar Cell	− 100	100	− 28.1	58.4	− 33.0	55.2	− 24.7	46.9	− 29.3	43.2	− 24.4	45.8	− 29.0	42.0	− 20.7	33.4	− 24.9	29.5
Solar Panel	− 40	125	− 31.5	56.6	− 32.7	53.4	− 31.0	44.3	− 31.3	40.5	− 30.5	43.2	− 31.0	39.3	− 24.3	30.1	− 24.6	26.0
Structure	− 40	80	− 24.8	43.3	− 30.0	39.2	− 23.8	40.3	− 28.6	36.3	− 23.6	39.6	− 28.3	35.5	− 20.0	34.2	− 24.3	30.9
Transceiver	− 20	60	− 19.4	16.2	− 25.4	10.6	− 18.7	14.6	− 24.3	9.4	− 18.5	14.3	− 24.1	9.1	− 16.4	10.6	− 21.5	5.7

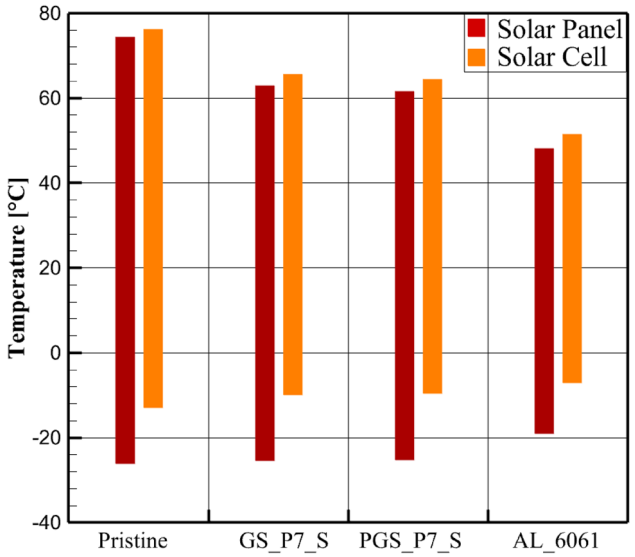

Fig. 6 Thermal analyses of the solar panels and solar cells in the hot transmit case

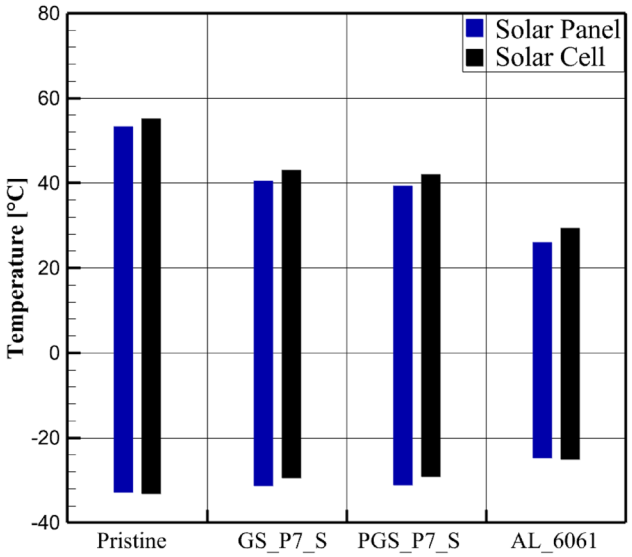

Fig. 8 Thermal analysis of solar panel and solar cell in cold survival case

and the temperature range was also the largest among the four cases. While the minimum temperature of the solar panel was -32.7 ˚C, the maximum and minimum temperatures of the solar cell were − 24.8 °C and − 33.0 °C, respectively. The solar panels with GS_P7_S and PGS_P7_S showed minimum temperatures of − 31.3 °C and − 31.0 °C, respectively, as shown in Figs. 8 and 9. The maximum and minimum temperatures of the solar cells with GS_P7_S were − 21.3 °C and − 29.3 °C, respectively. These were 3.5 °C and 3.7 °C higher compared to Pristine, respectively. The maximum and minimum temperatures of the solar cells with PGS_P7_S were − 21.2 °C and − 29.0 °C, which were 3.6 °C and 4.0 °C higher compared to Pristine, respectively. This shows that GS_P7_S and PGS_P7_S provided heat transfer paths inside the composite as GS and PGS, with high heat release between the carbon fiber prepregs, resulting in effective heat transfer performance. Finally, the minimum temperature of the aluminum-based solar panel was − 24.6 °C. Here, the maximum and minimum temperatures of the solar cell were − 20.7 °C and − 25.0 °C, respectively, showing the shortest temperature range.

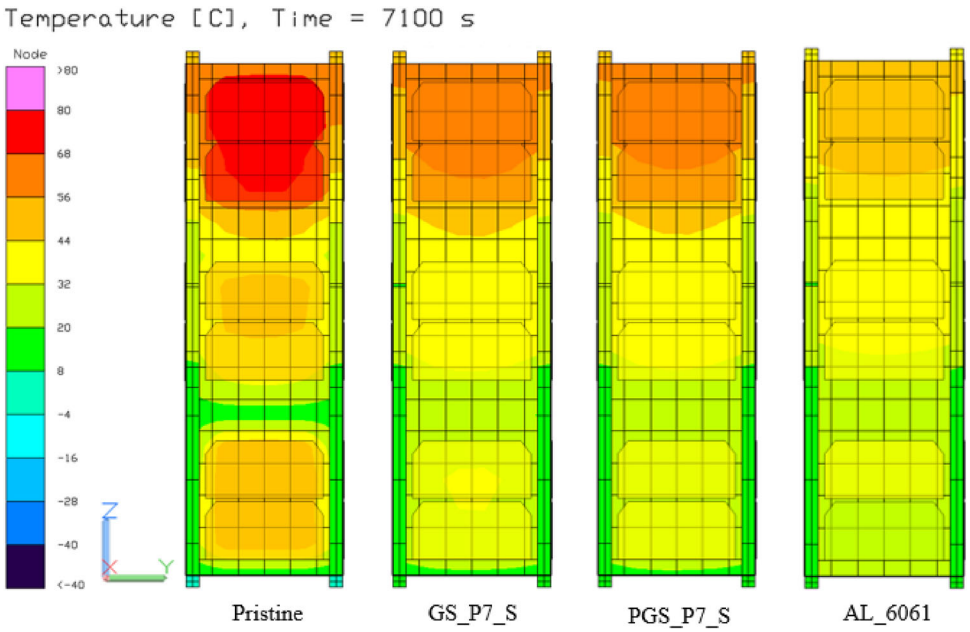

Fig. 7 Temperature distribution of the 3U solar panel at solar cell maximum temperature (*X* +)

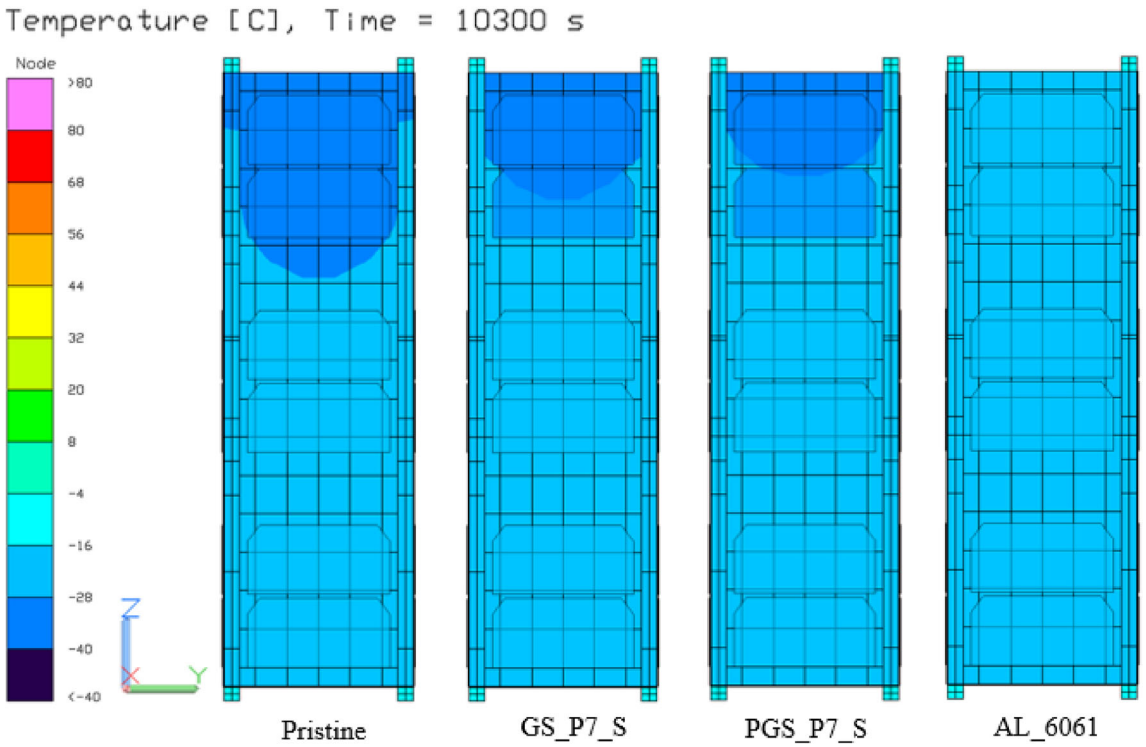

Fig. 9 Temperature distribution in the 3U solar panel at solar cell minimum temperature (Y +)

4.3 Comparative Analysis Based on Applied Materials

Tables 11 and 12 summarize the thermal conductivity, mechanical properties [42, 47], mass, worst hot, and worst cold case thermal analysis results for the Pristine solar panel in the 3U cube satellite, and with Aluminum6061-T6, and PGS_P7_S, a composite material with improved thermal conductivity.

First, when comparing Pristine and AL_6061, as shown in Table 11, the in-plane and thickness direction thermal conductivity of AL_6061 was 167.9 W/m·K, which is 7,137% and 28,357% higher than Pristine, respectively. However, the mechanical properties of AL_6061 showed that the specific strength was 114.3 kN·m/kg, which is 76.3% lower than Pristine. Additionally, the specific stiffness was 25.4 MN·m/kg, which is 42.1% lower compared to Pristine. The mass of the solar panel was 0.772 kg, an 86% increase compared to when Pristine was applied to the solar panel, and the total mass of the satellite was 3.715 kg, an increase of 10.6% compared to when Pristine was applied. The orbital thermal analysis results in the worst hot case showed that the maximum temperature of the transceiver, the component with the highest heat generation, was 44.1 °C, a 13.4% decrease compared to Pristine. The maximum temperature of the solar panel and cell was 48.1 and 51.5 °C, respectively, a decrease of 35.4% and 32.5% compared to Pristine, and it was confirmed that the temperature range was narrowly distributed.

The orbital thermal analysis results in the worst cold case showed that the lowest temperatures of the solar panel and cell were -24.6 and -25.0 °C, respectively, an increase of 24.8% and 24.2% compared to Pristine, and the temperature range was narrower than that of Pristine. Aluminum6061-T6 had excellent thermal properties compared to Pristine but relatively low mechanical properties. It has the disadvantage of having a larger mass than Pristine due to its high density.

Next, as shown in Table 12, when comparing Pristine and PGS_P7_S with their improved thermal conductivity, the thermal conductivity of PGS_P7_S in the plane and thickness direction was 34.2 and 38.7 W/m·K, respectively, which is an increase of 1,374% and 5,697%, respectively, compared to Pristine. However, the mechanical properties of PGS_P7_S were a specific strength of 149.9 kN·m/kg, which is 68.9% lower than Pristine. Additionally, the specific stiffness was 24.5 MN·m/kg, which is 44.2% lower compared to Pristine. Compared to AL_6061, the specific strength was 31.1% higher and the specific stiffness was 3.5% lower.

Consequently, the overall mechanical properties of PGS_P7_S were reduced compared to the Pristine. This reduction can be attributed to several factors: In PGS_P7_S, although the layers within the patterned region were bonded similarly to those in the Pristine, the presence of GS regions

Table 11 Comparison of Pristine and AL_6061 materials

	Pristine	AL_6061
Thermal Conductivity	Thermal conductivity in the plane and thickness direction is 2.32, 0.59 W/m·K	Thermal conductivity in the in-plane direction and thickness direction is 167.9 W/m·K, which is 7,137% and 28,357% higher than Pristine
Mechanical Properties [42, 47]	Tensile strength is 702 MPa, the tensile modulus of elasticity is 63.9 GPa The specific strength is 481.9 kN·m/kg, and the specific stiffness is 43.9 MN·m/kg	Tensile strength is 310 MPa, 55.8% lower than Pristine The tensile modulus of elasticity is 68.9 GPa, which is 7.82% higher than that of Pristine The specific strength is 114.3 kN·m/kg, a 76.3% decrease compared to Pristine The stiffness is 25.4 MN·m/kg, a 42.1% decrease compared to Pristine
Mass	The total mass of solar panels and satellites is 0.415 kg, 3.358 kg	The mass of the solar panel is 0.772 kg, an 86% increase compared to Pristine The satellite's total mass is 3.715 kg, a 10.6% increase compared to Pristine
Worst Hot Case	The maximum temperature of the transceiver is 50.9 °C The maximum temperature of solar panels and cells is 74.5 and 76.3 °C, respectively The temperature range of solar panels and cells is widely distributed	The maximum temperature of the transceiver is 44.1 °C, a 13.4% reduction compared to Pristine The maximum temperature of solar panels and cells is 48.1 and 51.5 °C, respectively, a 35.4% and 32.5% decrease compared to Pristine Compared to pristine, the temperature range of solar panels and cells is narrowly distributed
Worst Cold Case	The minimum temperature of solar panels and cells is − 32.7 and − 33.0 °C, respectively The temperature range of solar panels and cells is widely distributed	The minimum temperature of solar panels and cells is – 24.6 and − 25.0 °C, respectively, an increase of 24.8% and 24.2% compared to Pristine Compared to pristine, the temperature range of solar panels and cells is narrowly distributed

between layers decreased mechanical properties. Furthermore, the mechanical properties decreased due to damage and bending of the in-plane fibers caused by the insertion of stitching fibers.

The mass of the solar panel with PGS_P7_S was 0.460 kg, a 10.8% increase compared to Pristine, and the total mass of the satellite was 3.403 kg, an increase of 1.34% compared to Pristine.

The results of the orbital thermal analysis in the worst hot case showed that the maximum temperature of the transceiver was 47.9 °C, a 5.89% decrease compared to Pristine. The maximum temperature of the solar panel and cell was 61.8 and 64.5 °C, respectively, a decrease of 17.1% and 15.5% compared to Pristine, and it was confirmed that the temperature range was narrowly distributed. The orbital thermal analysis results in the worst cold case showed that the lowest temperatures of the solar panel and cell were -31.0 and -29.0 °C, respectively, which was an increase of 5.2% and 12.1% compared to Pristine, and the temperature range was narrower than that of Pristine.

PGS_P7_S improved the thermal performance of Pristine in the in-plane and thickness direction and was confirmed to have relatively excellent heat dissipation performance even in a space environment.

Additionally, comparing mechanical properties with AL_6061, the specific strength was 31.1% higher than that of AL_6061. Specific strength is the strength of a material divided by its density, indicating how much load it can withstand per unit weight. Therefore, PGS_P7_S demonstrated superior performance in terms of weight reduction.

5 Conclusions

In this study, PAN-carbon fiber-reinforced plastic (CFRP) with improved thermal conductivity was developed using a graphite sheet (GS), a patterned graphite sheet (PGS), and pitch-based carbon fiber stitching for weight reduction and efficient thermal control of a CubeSat. For verification, a thermal model of a 3U CubeSat was constructed and applied to solar panels. The micro-satellite was designed by simplifying it based on the 3U structure provided by ISISPACE, and it was assumed that the backing material determined the thermophysical and optical properties of the solar panel. In all cases, black anodizing was applied to the solar panel's internal and external optical properties to accurately compare thermal properties based on thermal conductivity. When Pristine, GS_P7_S, and PGS_P7_S materials were applied

Table 12 Comparison of Pristine and PGS_P7_S materials

	Pristine	PGS_P7_S
Thermal Conductivity	Thermal conductivity in the plane and thickness direction is 2.32, 0.59 W/m·K	Thermal conductivity in the in-plane direction and thickness direction is 34.2 and 38.7 W/m·K, respectively, an increase of 1,374% and 5,697%, respectively, compared to Pristine
Mechanical Properties [48]	Tensile strength is 702 MPa, the tensile modulus of elasticity is 63.9 GPa The specific strength is 481.9 kN·m/kg, and the specific stiffness is 43.9 MN·m/kg	Tensile strength is 242 MPa, a 65.5% decrease compared to Pristine The tensile elastic modulus is 39.5 GPa, a 38.2% decrease compared to Pristine The specific strength is 149.9 kN·m/kg, a 68.9% decrease compared to Pristine The stiffness is 24.5 MN·m/kg, a 44.2% decrease compared to Pristine
Mass	The total mass of solar panels and satellites is 0.415 kg, 3.358 kg	The mass of the solar panel is 0.460 kg, a 10.8% increase compared to Pristine The satellite's total mass is 3.403 kg, an increase of 1.34% compared to Pristine
Worst Hot Case	The maximum temperature of the transceiver is 50.9 °C The maximum temperature of solar panels and cells is 74.5 and 76.3 °C, respectively The temperature range of solar panels and cells is widely distributed	The maximum temperature of the transceiver is 47.9 °C, a 5.89% decrease compared to Pristine The maximum temperature of solar panels and cells is 61.8 and 64.5 °C, respectively, a decrease of 17.1% and 15.5% compared to Pristine Compared to Pristine, the temperature range of solar panels and cells is narrowly distributed
Worst Cold Case	The minimum temperature of solar panels and cells is − 32.7 and − 33.0 °C, respectively The temperature range of solar panels and cells is widely distributed	The lowest temperature of solar panels and cells is –31.0 and − 29.0 °C, respectively, an increase of 5.2% and 12.1% compared to Pristine Compared to Pristine, the temperature range of solar panels and cells is narrowly distributed

to the solar panel under these conditions, the total mass of the satellite was found to decrease by 9.60%, 9.02%, and 8.40%, respectively, compared to when Aluminum6061-T6 was used. Additionally, it was confirmed that the PGS_P7_S implemented in this study had a specific strength 31.1% higher than that of AL_6061. This verified the weight reduction achieved by the composite used in this study.

In-orbit thermal analysis was conducted to verify how effective the solar panels with three types of composites were for thermal control. The tendency in temperature distribution of the satellite payloads was determined based on the solar panel's material and the satellite's mode. In addition, the temperature distribution in the solar panels for the three cases of composites and the aluminum-based solar panel were compared and analyzed according to the satellite mode.

The thermal analysis results showed that GS_P7_S and PGS_P7_S effectively dispersed the heat generated inside the satellite compared to Pristine in the Worst Hot and Cold Cases, and also contributed to an improvement in the thermal stability of the satellite system, by promoting heat release into deep space. This was achieved via the heat transfer paths inside the composite material using GS, PGS, and stitching methods, which consequently demonstrated high heat dissipation performance. Accordingly, it was determined to exhibit effective heat transfer performance even in a space environment.

The composite material implemented in this study exhibited superior thermal properties compared to the existing CFRP. Still, it could not overcome the inherent mechanical property degradation due to GS's limitations and fiber damage during the stitching process [48]. In the future, research is needed to minimize the degradation of mechanical properties while maintaining a 3D heat transfer path. It is believed that this approach can contribute significantly to reducing the weight of satellites compared to aluminum.

Acknowledgements This work was supported by the National Research Foundation of Korea funded by the Ministry of Science and ICT under Grant (2022M1A3C2074536, Future Space Education Center).

Funding The funding has been received from National Research Foundation of Korea with Grant no. 2022M1A3C2074536.

Data availability The data supporting the findings of this study are available within the article.

Declarations

Conflict of Interest The authors declare none.

References

1. Kang SJ, Oh HU (2016) On-orbit thermal design and validation of 1U standardized CubeSat of STEP cube lab. Int J Aerosp Eng 2016:421389. https://doi.org/10.1155/2016/4213189
2. Kim JS, Kim HD (2022) Thermal model correlation and validation of a 6U nanosatellite with multiple payloads. Int J Aeronaut Space Sci 23:207–220. https://doi.org/10.1007/s42405-021-00409-4
3. Gilmore, David G (2002) Spacecraft thermal control handbook cryogenics. In: American Institute of Aeronautics and Astronautics
4. Fortescue P, Swinerd G, Stark J (2011) Spacecraft systems engineering. Wiley, New York
5. Meseguer J, Pérez-Grande I, Sanz-Andrés A (2012) Spacecraft thermal control. Elsevier, Amsterdam
6. Khalifa NS, Sharaf-Eldin TE (2013) Earth albedo perturbations on low earth orbit cubesats. Int J Aeronaut Space Sci 14(2):193–199. https://doi.org/10.5139/IJASS.2013.14.2.193
7. Roibas-Millan E, Alonso-Moragon A, Jimenez-Mateos AG, Pindado S (2017) Testing solar panels for small-size satellites: the UPMSAT-2 mission. Meas Sci Technol 28(11):115801. https://doi.org/10.1088/1361-6501/aa85fc
8. Tada HY, Charter JR, Anspaugh BE, Downing RG (1982) Solar cell radiation handbook, 3rd edn. NASA and JPL, USA
9. Baturkin V (2005) Micro-satellites thermal control—concepts and components. Acta Astronaut 56(1–2):161–170. https://doi.org/10.1016/j.actaastro.2004.09.003
10. Tachikawa S, Nagano H, Ohnishi A (2022) Advanced passive thermal control materials and devices for spacecraft: a review. Int J Thermophys 43(6):91. https://doi.org/10.1007/s10765-022-03010-3
11. Bhattarai S, Go JS, Kim H, Oh HU (2021) Development of a novel deployable solar panel and mechanism for 6U CubeSat of STEP cube lab-II. Aerospace 8(3):64. https://doi.org/10.3390/aerospace8030064
12. Kim SH, Joung YG, Seo BS, Yang JK, Park DH (2011) The design of 6-inch down-light by optimization of the optical and the thermal properties. Trans Korean Inst Electri Eng 60(6):1178–1182. https://doi.org/10.5370/KIEE.2011.60.6.1178
13. Lim LS, Bui TDV, Low KS, Tissera MSC, Pham VHP, Abhishek R, Soon JJ, Lew JM, Aung H, Goh ST, Chen SS (2016) VELOX-II: challenges of developing a 6U nanosatellite. Am Inst Aeronaut Astronaut Space 2016:5299. https://doi.org/10.2514/6.2016-5299
14. Shin KB, Kim CG, Hong CS, Lee HH (2001) Thermal distortion analysis of orbiting solar array including degradation effects of composite materials. Compos B Eng 32(4):271–285. https://doi.org/10.1016/S1359-8368(01)00020-8
15. Almehisni R, Al Naimat F (2018) Heat transfer influence of solar panel on spacecraft. Adv Sci Eng Technol Int Conf. https://doi.org/10.1109/ICASET.2018.8376815
16. Park TY, Chae BG, Kim H, Koo KR, Song SC, Oh HU (2021) New thermal design strategy to achieve an 80-kg-class lightweight X-band active SAR small satellite S-STEP. Aerospace 8(10):278. https://doi.org/10.3390/aerospace8100278
17. Budiantoro PA, Fauzi A, Ramayanti S, Fitrianingsih E, Nasser EN, Suryanti DI, Slamet W (2022) Thermal design and analysis of deployable solar panel low earth orbit equatorial constellation satellite. In: 2022 IEEE International Conference on Aerospace Electronics and Remote Sensing Technology, pp. 1–7.https://doi.org/10.1109/ICARES56907.2022.9993478
18. Jun HY, Kim JH, Park JS (2011) Analysis of satellite panel using carbon composites. Aerosp Eng Technol 10(2):114–120
19. Heidt H, Puig-Suari J, Moore A, Nakasuka S, Twiggs R (2000) CubeSat: a new generation of picosatellite for education and industry low-cost space experimentation. In: Small Satellite Conference
20. Villela T, Costa CA, Brandão AM, Bueno FT, Leonardi R (2019) Towards the thousandth CubeSat: a statistical overview. Int J Aerosp Eng 1:5063145. https://doi.org/10.1155/2019/5063145
21. Kang MG, Kim DH, Jang DI, Lee H, Myong RS (2023) Thermal flow field analysis of heat sink for improving cooling efficiency. Korean Soc Comput Fluids Eng 28(3):83–91. https://doi.org/10.6112/kscfe.2023.28.3.083
22. Lee JY, Huh HI, Kim SH, Chang SY, Lee DG, Lee SH, Choi HJ (2011) Preliminary thermal analysis for LEO satellite optical payload's thermal vacuum test. J Korean Soc Aeronaut Space Sci 39(5):466–473. https://doi.org/10.5139/JKSAS.2011.39.5.466
23. Kim GN, Kim CH, Chung K, Han JH, Gilles F (2002) Thermal analysis of composite satellite antenna structure in space environment 77–80. In: Proceedings of the Korean Society for Composite Materials Conference
24. Han S, Chung DDL (2011) Increasing the through-thickness thermal conductivity of carbon fiber polymer–matrix composite by curing pressure increase and filler incorporation. Compos Sci Technol 71(16):1944–1952. https://doi.org/10.1016/j.compscitech.2011.09.011
25. Ren L, Kang L, Niu H, Guo H, Lv R, Bai S, Li M (2022) Structural optimization design of CFRP with ultrahigh in-plane thermal conductivity and mechanical strength. Compos A Appl Sci Manuf 163:107209. https://doi.org/10.1016/j.compositesa.2022.107209
26. Cho HK, Rhee J (2011) Vibration in a satellite structure with a laminate composite hybrid sandwich panel. Compos Struct 93(10):2566–2574. https://doi.org/10.1016/j.compstruct.2011.04.019
27. Idris MK, Naderi P, Melenka GW, Grau G (2021) Damage location sensing in carbon fiber composites using extrusion printed electronics. Funct Compos Struct 3(4):045001. https://doi.org/10.1088/2631-6331/ac3731
28. Emrahi R, Rostamiyan Y, Hashemi-Tilehnoee M (2023) Influences of nano-SiO_2 on the tensile, flexural, and compressive characteristics of the open-hole carbon fiber-reinforced polymer laminated composites: an experimental study. Funct Compos Struct 5(3):035001. https://doi.org/10.1088/2631-6331/ace3a1
29. Cha J, Yoon S (2022) Determination of shift factor for long-term life prediction of carbon/fiber epoxy composites using the time-temperature superposition principle. Funct Compos Struct 4(1):015003. https://doi.org/10.1088/2631-6331/ac529e
30. Lee JS, Jo H, Choe HS, Lee DS, Jeong HJ, Lee HR, Kweong JH, Lee H, Myong RS, Nam YW (2022) Electro-thermal heating element with a nickel-plated carbon fabric for the leading edge of a wing-shaped composite application. Compos Struct 289:115510. https://doi.org/10.1016/j.compstruct.2022.115510
31. Kang YS, Park SW, Roh JS, Myong RS (2021) Computational investigation of effects of expanded metal foils on the lightning protection performance of a composite rotor blade. Int J Aeronaut Space Sci 22:203–221. https://doi.org/10.1007/s42405-020-00288-1
32. Abdelal GF, Atef A (2008) Thermal fatigue analysis of solar panel structure for micro-satellite applications. Int J Mech Mater Design 4:53–62. https://doi.org/10.1007/s10999-008-9057-3
33. Li J, Yan S, Cai R (2013) Thermal analysis of composite solar array subjected to space heat flux. Aerosp Sci Technol 27(1):84–94. https://doi.org/10.1016/j.ast.2012.06.010
34. Park TY, Kim SY, Yi DW, Jung HY, Lee JE, Yung JH, Oh HU (2021) Thermal design and analysis of unfurlable CFRP skin-based parabolic reflector for spaceborne SAR antenna. Int J Aeronaut Space Sci 22:433–444. https://doi.org/10.1007/s42405-020-00301-7
35. McDonald PC, Jaramillo E, Baudouy B (2006) Thermal design of the CFRP support struts for the spatial framework of the Herschel space observatory. Cryogenics 46(4):298–304. https://doi.org/10.1016/j.cryogenics.2005.12.001

36. Kim RY, Crasto AS, Schoeppner GA (2000) Dimensional stability of composite in a space thermal environment. Compos Sci Technol 60(12–13):2601–2608. https://doi.org/10.1016/S0266-3538(00)00052-X
37. Noorunnisa Khanam P, Abdul Khalil HPS, Jawaid M, Ramachandra Reddy G, Surya Narayana C, Naidu V (2010) Sisal/carbon fiber reinforced hybrid composites: tensile, flexural and chemical resistance properties. J Polym Environ 18:727–733. https://doi.org/10.1007/s10924-010-0210-3
38. Yu GC, Wu LZ, Feng LJ (2015) Enhancing the thermal conductivity of carbon fiber reinforced polymer composite laminates by coating highly oriented graphite films. Mater Des 88:1063–1070. https://doi.org/10.1016/j.matdes.2015.09.096
39. Li M, Fang Z, Wang S, Gu Y, Zhang W (2021) Thermal conductivity enhancement and synergistic heat transfer of z-pin reinforced graphite sheet and carbon fiber hybrid composite. Int J Heat Mass Transf 171:121093. https://doi.org/10.1016/j.ijheatmasstransfer.2021.121093
40. An WJ, Park GY, Choi JH (2020) Process variables of I-fiber stitching in mode I failure. Compos Struct 240:11082. https://doi.org/10.1016/j.compstruct.2020.112082
41. ASTM Committee E37 on Thermal Measurements (2007) Standard test method for determining thermal diffusivity by the flash method. ASTM International.
42. Kissell J, Randolph R, Ferry L (2002) Aluminum structures: a guide to their specifications and design. Wiley, New York
43. ASTM standard D3039/D3039M (2004) Standard test method for tensile properties of polymer matrix composite materials. ASTM International
44. Modest MF, Mazumder S (2021) Radiative heat transfer. Academic Press, Cambridge
45. Cullimore B, Ring S, Johnson D (2004) SINDA/FLUINT user's manual. C&R Technologies, Littleton.
46. Lee ST, Lee SH, Choi YJ, Lew JH (1997) Development of altitude control thruster for KOMPSAT. J Korean Soc Propul Eng 1:67–73. https://doi.org/10.6108/KSPE.2020.24.5.091
47. Foster I (2022) Small satellite thermal modeling guide. Albuquerque: Kirtland Air Force Base
48. Park GB, Kang YH, Kim DJ, Nam YW, Kwak BS (2024) Thermal and mechanical behavior of multifunctional carbon/epoxy composite with patterned graphite sheet and stitched pitch-based carbon fiber. In Review.